UCRL-JC-127288 Pt 1
PREPRINT

# Diamond Radiation Detectors
# I. Detector Properties for IIa Diamond

Don R. Kania

This paper was prepared for submittal to the
Proceedings of the International Summer School of Physics
"Enrico Fermi"
Bologna, Italy
July 30-August 2, 1996

May 16, 1997

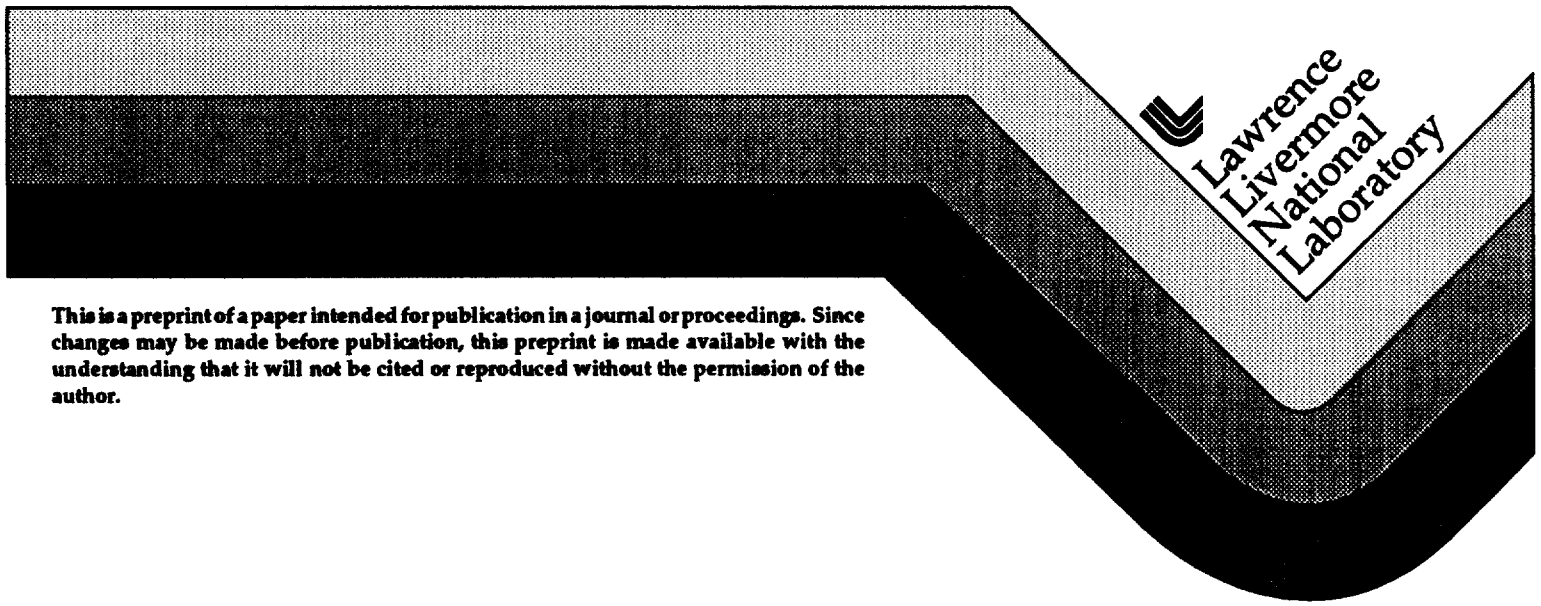

VA-PA 135-8



# Diamond radiation detectors

## I. – Detector properties of IIa diamond

D. R. KANIA

*Advanced Microtechnology Program, Lawrence Livermore National Laboratory Livermore, CA 94551*

as soon as possible - Thanks

## 1. – Introduction

Diamond radiation detectors have a lengthy history. Photoconductive ultraviolet detectors were developed in the 1920's and ionizing radiation detectors were fabricated in the 1940's. However, these devices found only restricted usage due to the limitations of geological diamonds. Specifically, the limitations of geological diamond are small size and uncontrolled material characteristics. Advances in the quality and size of CVD diamonds have created new opportunities for the fabrication and application of diamond radiation detectors. In particular, fast, radiation hard, diamond detectors for high-energy physics experiments has become a near-term possibility.

Diamond is a very interesting material with many extreme properties. For application to radiation detectors, the large bandgap, radiation hardness, optical transparency, large saturated carrier velocities and low atomic number are important properties of diamond. In this lecture we will restrict our discussion to radiation detectors in the form of two-terminal devices with a MSM (metal-semiconductor-metal) structure. The semiconductor is undoped diamond. The metal contacts are ohmic, no junctions are used. We will be discussing the simplest diamond devices.

Any radiation that generates free carriers in diamond can be detected. This includes photons with an energy greater than the bandgap of 5.5 eV which includes ultraviolet, X-ray and gamma rays. High-energy particles can also be detected: alpha-particles, electrons, neutrons, pions, etc. The transport and collection of the generated charge can be described independent of the type of the exciting radiation. We will focus our attention on the transport of the free charges created by the incident radiation moving in the electric field applied across the diamond. These drifting free charges, electrons and holes, generate a current in the external circuit. An excellent review of the basic physics of the interaction of radiation with matter, charge generation, is found in Knoll [1].

## 2. – Radiation detection

A MSM diamond detector is a high-resistivity diamond sandwiched between two metal electrodes. An external voltage is applied to the metal contacts generating an electric field across the device. The basic physics can be illustrated by assuming a uniform device with one mobile charge carrier, electron or hole, generated by the incident radiation. The charges are generated at a rate $g(t)$. The generation rate is proportional to the intensity of the absorbed radiation per unit volume divided by the average energy to form a free charge (electron-hole pair), $\gamma$. A rough estimate for $\gamma$ is three times the bandgap energy for particle with an energy much greater than the bandgap. For energies near the band edge, one quantum produces one electron-hole pair. The number of charges is related to the generation rate by the following

$$\mathrm{d}n/\mathrm{d}t = g(t) - n/\tau \,, \tag{1}$$

where $\tau$ is the carrier lifetime, free charge is lost or trapped by a random process. The lifetime may be limited by defects or the device geometry. For an impulse excitation,

$$n(t) = n_0 \exp[-t/\tau]$$

and $n_0$ is the carrier density at $t = 0$. In the steady state, $n = \tau g$. The current density is

$$j = env \,,$$

where $e$ is the electric charge, $v$ is the carrier velocity $v = \mu(E)\, E$. The electric field is $E$ and $\mu$ is the carrier mobility. The sensitivity, usually in the units of ampere of current per watt of radiation absorbed, of a detector can be written in terms of the applied voltage (electric field), $E = V/L$, as

$$S = e\mu\tau V/\gamma L^2 = e\mu\tau E/\gamma L \,.$$

Note the inverse scaling with the dimension of the detector along the electric-field direction.

The charge collection time or transit time is $L/v$, where $L$ is the length of the device along the electric field. The charge or integrated current generated in the external circuit is

$$q = Qv\tau/L = Qd/L \,,$$

where $Q$ is the total charge generated in the detector and $d$ is the mean distance a charge moves in the detector. Note, a charge need not reach a contact to generate current or charge in the circuit, this is known as the Ramo-Shockley theorem [2] which follows directly from Gauss's law.

If $d > L$, then all of the charge will be detected. If $d < L$, only a fraction of $Q$ will be detected. In the case of incomplete charge collection, care must be taken in the design of the device to eliminate the effects of space charge build-up. The uncollected charge

within device can result in the accumulation of a localized net charge within the device which will distort the electric-field distribution within the device. This typically manifests itself as reduced detection efficiency.

From this analysis we can see that the important material parameters are the mobility and lifetime of the charge carriers or their product, $d = \mu\tau E$. A generalization to electron and hole conduction is trivial where each parameter becomes a sum of the electron and hole contributions. For example, $d = d_e + d_h$, while the lifetime and mobility add as a weighted inverse, $\mu \equiv (\mu_n \tau_n + \mu_h \tau_h)/\tau$. This analysis is extremely simplified and can be found in greater depth in Bube [3] and Zhao [4].

## 3. – Properties of diamond

Although silicon, the most common detector material, will not be replaced by diamond, it does possess many inherent advantages, for specific applications. As previously mentioned, the high resistivity of intrinsic diamond eliminates the need for reverse-biased junctions and the associated material doping to suppress thermally generated currents. The leakage currents and their fluctuations are an undesirable noise source in radiation measurements and limit the magnitude of the electric field.

TABLE I. – *Properties of diamond and silicon.*

| Property | Diamond | Silicon |
|---|---|---|
| density (g/cm$^3$) | 3.5 | 2.32 |
| bandgap (eV) | 5.5 | 1.1 |
| resistivity ($\Omega$ cm) | $> 10^{12}$ | $10^5$ |
| breakdown voltage (V) | $10^7$ | 1000 (*pn* junction) |
| electron mobility (cm$^2$V/s) | 1800 | 1500 |
| hole mobility (cm$^2$V/s) | 1200 | 480 |
| saturation velocity ($\mu$m/ns) | 220 | 100 |
| dielectric constant | 5.6 | 11.7 |
| energy to form electron-hole pair (eV) | 13 | 3.6 |
| atomic number | 6 | 14 |
| average minimum ionizing particle signal in 100 $\mu$m (electrons) | 3600 | 8900 |

The low dielectric constant of diamond reduces the capacitance of a diamond detector, a potential source of speed and noise improvement. The large bandgap of diamond significantly reduces the detector sensitivity to visible radiation (ignoring defects) and contributes to its radiation hardness.

As previously mentioned, the high resistivity of intrinsic diamond eliminates the need for reverse-biased junctions to suppress thermally generated currents. The leakage currents and their fluctuations are an undesirable noise source in radiation measurements and limit the magnitude of the electric field. The low dielectric constant of diamond reduces the capacitance of a diamond detector, a potential source speed and noise improvement. The large bandgap of diamond significantly reduces the detector sensitivity to visible radiation (ignoring defects) and contributes to its radiation hardness.

The high saturated carrier velocity permits high-speed and high-count-rate operation of diamond detectors. This characteristic is especially important in high-count-rate applications. The low atomic number can be and advantage in two ways: 1) reducing high-energy cascades in high-energy particle experiments and 2) the absorption characteristics are well matched to human soft tissue. This is an important property for radiation dosimetry applications. The low $z$ of diamond is a disadvantage in other applications where it reduces the stopping power of the radiation of interest, reducing the sensitivity of the detector. For minimum ionizing particles, this is greater than a factor of two relative to silicon.

## 4. – History

We will briefly review the history of diamond detectors, a more extensive review can be found in Kania [5]. The use of diamond as a radiation detector has its origins early in this century. Gudden and Pohl in 1923 used a photoconductive detector to study the absorption characteristics of diamond [6]. Hofstadter reviewed the work on natural diamond "crystal counters" for nuclear radiation in 1949 [7].

Other researchers studied the interaction of high-energy electrons and alpha-particles through the 1950's and 60's. Detectors improved with the work of Konorova and Kozlov [8] which showed how to eliminate space charge effects using injecting contacts. The application to human-tissue dosimetry was explored by many authors. High-speed photoconductors were developed by Kania *et. al.* for UV and soft X-rays [9]. Recent work has focused on detectors for use in high-energy physics experiments [10].

## 5. – Detector characteristics of IIa diamond

The carrier transport properties, $\mu$ and $\tau$, of IIa diamonds have been studied for a long time. We will briefly review these properties. More extensive analysis can be found in the lecture by Collins in this volume and in Pan and Kania [11].

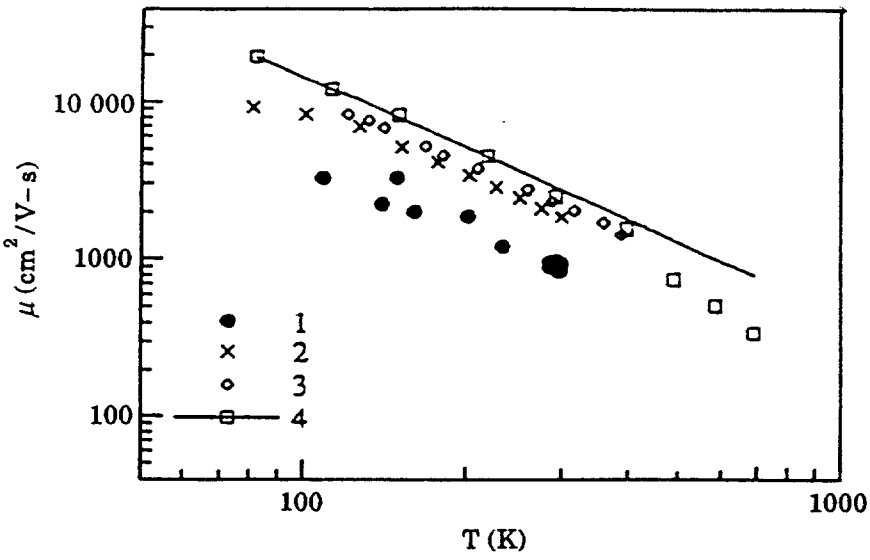


Fig. 1. – Electron mobility *vs* temperature - 1. Klick and Maurer (1951), 2. Redfield (1954), 3. Konorova (1967), 4. Nava (1979). The line represents a $T^{-3/2}$ fit.

The large mobility of both and electrons and holes is a key property of diamond in detectors. The high mobility is a partial consequence of the high Debye temperature and inelasticity of the material. At low electric fields the mobility is independent of the electric field. As the electric field increases beyond $10^4$ V/cm, the velocity saturates. In non-polar semiconductors, like diamond, acoustic phonons and ionized impurities are the dominant sources of scattering. At temperatures between about 200 and 500 °C, *phonon* scattering dominates, scaling as $T^{-3/2}$. At lower temperatures, ionized impurity scattering can dominate. This mechanism scales at $T^{3/2}$. At room temperature and low electric fields, the electron mobility is 1800 $cm^2$ V/s and the hole mobility is 1200 $cm^2$ V/s for the very best samples, significant sample-to-sample variability is to be expected. A compilation of electron mobility data is shown in fig. 1.

At low electric fields the average kinetic energy of the electrons and holes is close to $3/2\,kT$. As the field increases, the energy gained by the carriers becomes large enough to generate optical phonons. This energy loss mechanism causes the velocity to saturate. The saturation velocity $v_s$ can be expressed as

$$v_s = (8E_{opt}/3\pi m)^{1/2},$$

where $E_{opt}$ is the longitudinal optical-phonon energy of 163 meV and $m$ is the density-of-states effective mass. This effect has been measured by Nava *et. al.* [12]. This effect leads to a saturation in $d$ at high electric fields as shown in fig. 2. This sample had a $d$ of 50 $\mu$m near saturation [13]. Significant variability is seen from sample to sample. A reasonable range for $d$ is 20 to 50 $\mu$m.

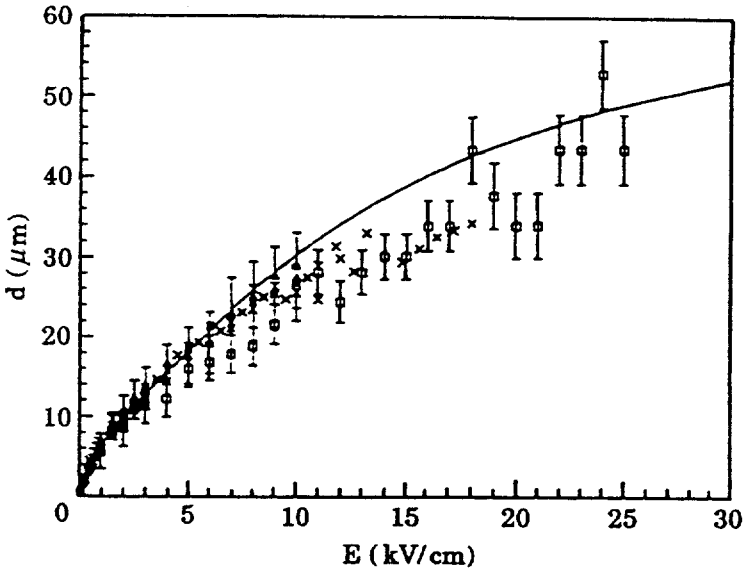


Fig. 2. – Collection distance measured as a function of the applied electric field in IIa diamond. Ionizing radiation (× and □) and photoconductivity (▲ and ●) data are used.

At carrier densities greater than $10^{16}\,\mathrm{cm}^{-3}$, an additional scattering mechanism effecting the mobility must be included. At these high densities electron and holes can scatter off of each other in analogy to impurity scattering. The theoretical modeling of the effect was first developed for silicon [14]. The effect on mobility scales roughly as $T^{3/2}(np)^{-1/2}$. This effect can be quite dramatic, reducing the low excitation density mobility by a factor of 1000 at a density of $10^{18}\ \mathrm{cm}^{-3}$.

The carrier lifetime in type IIa diamond has been measured by several groups [15]. These measurements typically measure the lifetime of electrons and holes together in radiation excitation-decay experiments. The lifetime typically varies from 1 ns to 100 ps. This parameter is very sample dependent. Reference [12] noted that the lifetime was inversely correlated with the nitrogen concentration of the diamonds. This suggests that nitrogen, a deep donor, acts as a trap in diamond. The lifetime should scale as

$$\tau = (N\langle\sigma v\rangle)^{-1},$$

where $N$ is the concentration of the trapping site, $\sigma$ is the trapping cross-section and $v$ is the thermal velocity. The brackets denote a thermal average over the cross/section. This is the quality used in eq. (1). This description is easily generalized to individual lifetimes for electrons $\tau_e$ and holes $\tau_n$. Finally, there are several examples of extraordinary samples in the literature indicating lifetimes well in excess of 10 ns and collection distances in excess of 150 μm [16].

Band-to-band recombination has a cross-section of $10^{-19}$ cm$^{-2}$ and can be ignored. It is much smaller than the cross-section for charged-center trapping which is of order $10^{-14}$ cm$^{-2}$ or neutral-site trapping which is of order $10^{-16}$ cm$^{-2}$.

## 5. – Rate equation modeling

The analysis based upon eq. (1) is referred to as the single-carrier model. In this model only one carrier is considered with a single trap. Photoconductive experiments performed by Pan *et al.* showed significant deficiency in this model [17]. Pan developed a more sophisticated model which consistently included separate trapping dynamics for electrons and holes coupled by a nitrogen trapping center. The modeling of the mobility included the effects of electron-hole scattering.

The nitrogen trap is characterized as a deep donor, its initial ionization is extremely low. In the model, all nitrogen is assumed to be unionized before excitation. The details of the site, whether it is single substitutional or and aggregate, are irrelevant to the

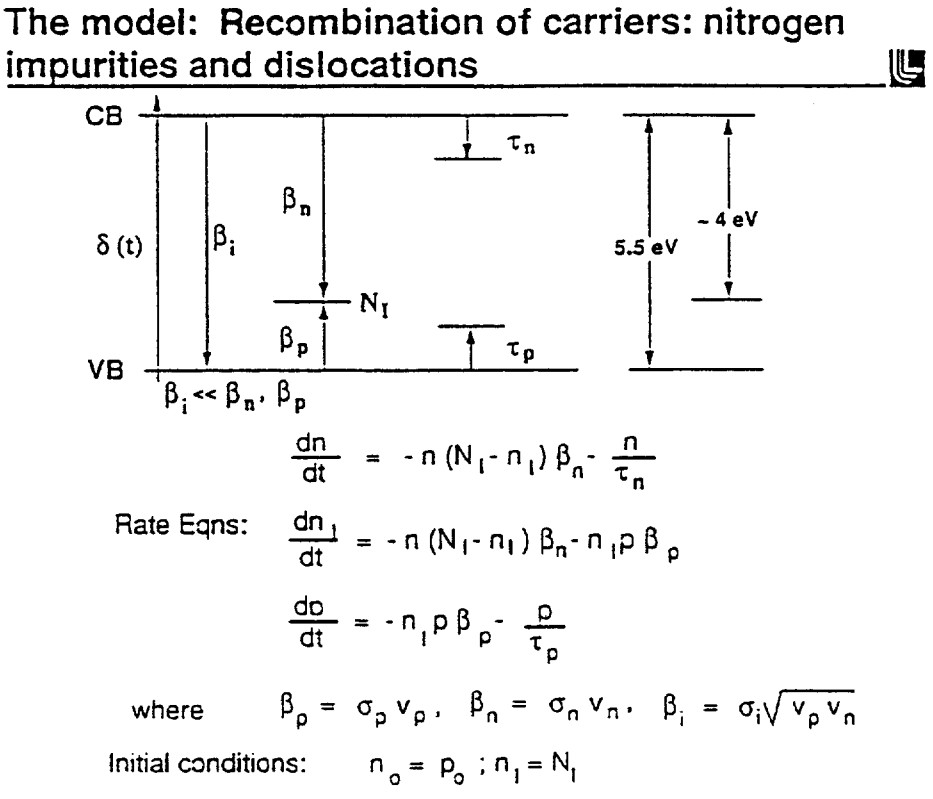


Fig. 3. – A schematic of the rate equation model.

modeling. The carrier dynamics are modeled by three rate equations

$$dn/dt = g(t) - n(N_1 - n_1)\langle\sigma v\rangle_n - n/\tau_\varepsilon \quad \text{for electrons,}$$
$$dn/dt = g(t) - pn_1\langle\sigma v\rangle_h - p/\tau_p \quad \text{for holes and}$$
$$dn_1/dt = n(N_1 - n_1)\langle\sigma v\rangle_n - pn_1\langle\sigma v\rangle_h \quad \text{for the nitrogen traps.}$$

$N_1$ is the nitrogen concentration, $n_1$ is the density of neutral nitrogen sites. A schematic of this model is shown in fig. 3.

This model was used to simulate transient photoconductivity experiments. This photon source for these experiments was a frequency pentupled YAG laser yielding photons of 6.11 eV. The laser was powerful enough to excite a carrier density of near $10^{19}\,cm^{-3}$. Sample data are shown in fig. 4. Two density-dependent effects are evident in the data. First, the amplitude does not scale with density or illumination intensity. Second, the decay time is a function of the excitation density.

The best-fit parameters for one sample from the model calculations are summarized in table II.

The modeling fits the measured decay times extremely well (see fig. 5) and accurately the photoconductive signals over 5 orders of magnitude of excitation density. Although the mobilities are smaller than one might expect, the other

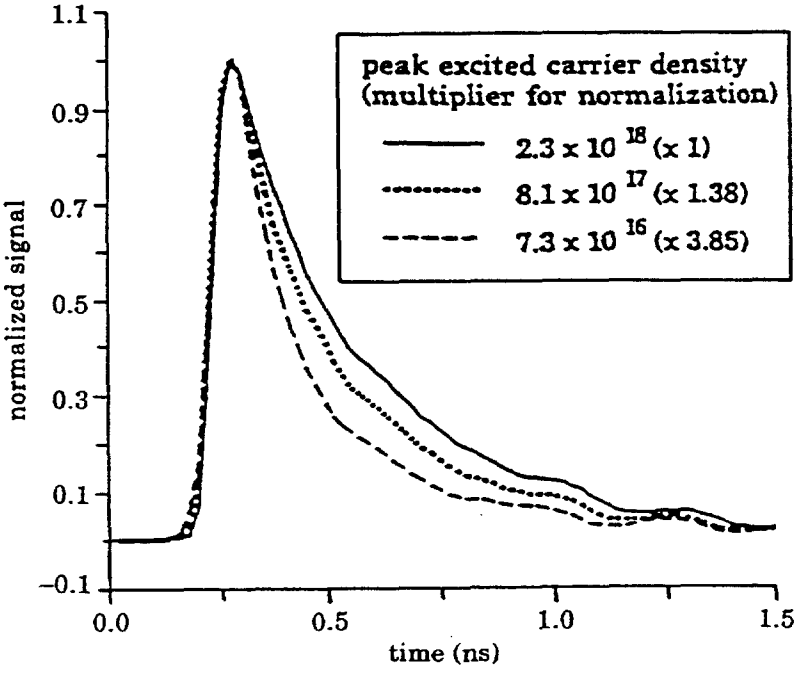


Fig. 4. – Photoconductive signals at three different peak carrier densities normalized to the largest signal.

TABLE II. – *Model parameters.*

| Parameter | Electrons | Holes |
|---|---|---|
| $\mu_0$(cm$^2$ V/s) | 370 | 260 |
| $\tau$ (ps) | 230 | 230 |
| $\sigma$ (cm$^{-2}$) | $3 \times 10^{-14}$ | $1 \times 10^{-16}$ |
| $N_1$ (cm$^{-3}$) | $3.4 \times 10^{18}$ | — |

parameters are consistent with our expectations. The electron and hole trapping cross-sections are consistent with a charged and a neutral site, respectively. The nitrogen density is consistent with absorption based measurements of the nitrogen density of 20 p.p.m. We must note that the model includes $\tau_n$ and $\tau_p$ which represent uncoupled traps for electrons and holes. These states are required to fit the data. Their nature is unknown, we speculate they may represent trapping at dislocations or vacancies.

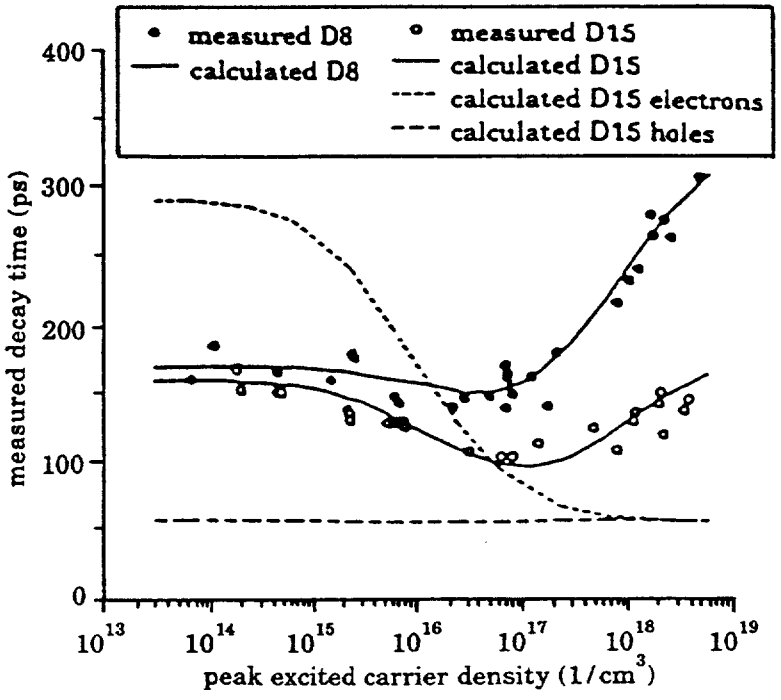


Fig. 5. – Photoconductive decay time as a function of the carrier density for two different samples. The lines through the points are the results of the calculations.

Examining the dynamics in the calculation, we see that the holes decay quickly because of the high density of neutral nitrogen sites. The electrons decay slowly at low density. As the intensity increases, the hole decay is unaffected, but the electron lifetime decreases as charged nitrogen sites are generated by the holes.

This type of modeling can provide a guide to designing diamond radiation sensors. The effects of temperature, electric field, impurity concentration, excitation density and geometry can be included with a minimum of *ad hoc* parameters. Again we note that the sample-to-sample variability can be large. Experimental tests are required.

## 6. – Conclusions

The detector properties and carrier dynamics of type IIa diamonds are reasonably well understood. The trends in the electron and hole mobilities have been characterized as a function of temperature, impurity content, electric field and carrier density. The carrier lifetimes are coupled through the nitrogen impurity. This leaves us with typical samples with collection distances of 20 to 50 $\mu$m. The detailed dynamics of the carriers can be modeled using a rate equation analysis. Much progress has been made in understanding the detector properties of diamond, but continued progress has been limited by the geologic processes used to make the material, *i.e.* limited sample size and no synthesis control. CVD diamond promises to eliminate these restrictions. This will be discussed in the next lecture.

## REFERENCES

[1] KNOLL G. F., *Radiation Detection and Measurement* (John Wiley and Sons, New York, N. Y.) 1989.
[2] RAMO S., *Proc. IRE*, 27 (1939) 584.
[3] BUBE R. H., *Photoconductivity of Solids* (John Wiley and Sons, New York, N.Y.) 1960.
[4] ZHAO S., *Characterization of the Electrical Properites of Polycrystalline Diamond Films*, Ph.D. Thesis, Ohio State University, 1994.
[5] KANIA D. R., *Diamond Radiation Detectors*, Proc. ICNDST 1992, Heidelberg.
[6] GUDDEN B. and POHL R., *Z. Phys.*, 17 (1923) 331.
[7] HOFSTADTER R., *Nucleonics*, April, 2 (1949).
[8] KONOROVA E. A. and KOZLOV S. F., *Sov. Phys. Semicond.*, 4 (1971) 1600.
[9] KANIA D. R. *et al.*, *Rev. Sci. Instrum.*, 27 (1990) 2765.
[10] FRANKLIN M. *et al.*, *Nucl. Instrum. Methods A*, 315 (1992) 39.
[11] PAN L. and KANIA D. R., *Diamond: Electronic Properties and Applications* (Kluwer Academic Publishers, Boston, Mass.) 1995.
[12] NAVA F. *et al.*, *IEEE Trans. Nucl. Sci.*, NS-26 (1979) 308.
[13] PAN L. S. *et al.*, *J. Appl. Phys.*, 74 (1993) 1086.
[14] CHOO S. C., *IEEE Trans. Electron. Dev.*, ED-19 (1954) 1525.
[15] KONOROVA E. A., KOZLOV S. F. and VAVILOV V. S., *Sov. Phys. Solid State*, 8 (1966) 1.
[16] PAN L. S. *et al.*, *MRS Meeting-Spring 1993* (San Francisco, Cal.).
[17] PAN L. S. *et al.*, *Appl. Phys. Lett.*, 57 (1990) 623.

**This work was performed under the auspices of the U.S.Department of Energy by Lawrence Livermore National Laboratory under contract no. W-7405-Eng-48.**

*Technical Information Department* • **Lawrence Livermore National Laboratory**
**University of California • Livermore, California 94551**